Palaeogeography, Palaeoclimatology, Palaeoecology 333-334 (2012) 148–159

Contents lists available at SciVerse ScienceDirect

Palaeogeography, Palaeoclimatology, Palaeoecology

journal homepage: www.elsevier.com/locate/palaeo

The annual particle cycle in Lake Van (Turkey)

Mona Stockhecke [a,*], Flavio S. Anselmetti [a], Aysegül F. Meydan [b], Daniel Odermatt [c], Michael Sturm [a]

[a] Eawag, Swiss Federal Institute of Aquatic Science and Technology, Department of Surface Waters Research and Management, Ueberlandstrasse 133, P. O. Box 611, 8600 Dübendorf, Switzerland
[b] Yüzüncü Yıl Üniversitesi, Mühendislik-Mimarlık Fakültesi, Jeoloji Mühendisliği Bölümü 65080, Van, Turkey
[c] Remote Sensing Laboratories, Department of Geography, University of Zurich, Winterthurerstrasse 190, 8057 Zurich, Switzerland

ARTICLE INFO

Article history:
Received 1 September 2011
Received in revised form 2 March 2012
Accepted 13 March 2012
Available online 19 March 2012

Keywords:
Sequential sediment traps
Satellite data
Seasonal particle fluxes
Annually laminated sediment
Lake Van
Sedimentary archive

ABSTRACT

The varved sediments of Lake Van provide a high-quality continental archive of seasonal to decadal-scale climate variability. In order to read the natural record, modern varve formation was studied on the basis of (1) remotely-sensed total suspended-matter (TSM_{rs}) concentrations; (2) time-series of particle flux and water temperatures; and (3) turbidity, temperature, and oxygen profiles. TSM_{rs}, validated by contemporaneous water-column sampling, shows great temporal and lateral variations (whitings and turbidity plumes). From 2006 to 2009, sequential sediment traps recorded high particle fluxes during spring and fall, medium fluxes during summer, and almost zero flux during winter. The mean total mass flux of 403 mg m^{-2} day^{-1} comprised 33% (seasonally up to 67%) calcium carbonate, 7% aquatic organic matter, 6% biogenic opal, and 54% detrital minerals. The $CaCO_3$ fluxes are controlled by river discharge (precipitation and snowmelt) during spring, by high productivity during summer, and by river discharge (precipitation before snowfall starts) and mixing during fall. In November 2007, an anomalously high $CaCO_3$ flux occurred as a result of a warm water surface supersaturated with calcite coinciding with an anomalous runoff event. The results demonstrate that the couplets of light and dark laminae in the short sediment cores are true varves representing spring–summer–fall and winter conditions, respectively. Consequently, varve formation can be linked to the seasonal climate pattern, providing a calibration that can be used to interpret the partially varved paleo-record of Lake Van and related environmental processes.

1. Introduction

Annually laminated lacustrine sediments ('varves' after de Geer, 1910) are natural, paleoenvironmental archives containing high-resolution proxy data and precise chronologies that can be used to study seasonal to decadal-scale climate variability (Brauer et al., 2008; Fig. 1). Closed-basin lakes are particularly well-suited for such studies. Assuming no groundwater interaction, the levels of such lakes are sensitive only to climate (evaporation, precipitation, and river inflow), which also strongly affects sedimentation processes. Lake Van in eastern Anatolia (Turkey), a closed-basin lake located in a transitional zone between major atmospheric circulation systems, represents an excellent continental archive to investigate the evolution of the Quaternary climate in the Near East. Because of its potential, Lake Van was designated a key site within the International Continental Scientific Drilling Program (ICDP) (Litt et al., 2009). In 2010, its sedimentary subsurface was drilled as part of the Paleovan project and varved sedimentary successions were recovered that span several glacial–interglacial cycles (Litt et al., 2011).

In order to fully exploit the potential of Lake Van's varved sediments, knowledge of the sedimentological response of the lake to the prevailing weather and climate conditions is required (Thunell et al., 1993; Broecker, 2002). A powerful approach involves monitoring modern sediment deposition in the lake basin and relating it to meteorological and limnological variables (Lotter and Birks, 1997; Lotter et al., 1997; Kienel et al., 2005). Sediment-trap studies yield valuable information about vertical and temporal particle dynamics (Sturm et al., 1982; Teranes et al., 1999; Douglas et al., 2002), while remote-sensing instruments yield information on the horizontal distribution of particles at high temporal resolution (Odermatt et al., 2009; Lahet and Stramski, 2010; Matthews et al., 2010). Seasonal sediment fluxes reflect the environmental conditions prevailing in both the water column and the catchment. This is because the flux of autochthonous particles (e.g., carbonate, diatoms) is affected by the conditions pertaining in the water column, while the flux of allochthonous particles (e.g., detrital minerals, pollen) is affected by the conditions pertaining in the catchment. In Lake Van, autochthonous carbonate precipitation in the epilimnion is recognizable as drifting, milky clouds, termed whitings (Strong and Eadie, 1978; Shinn et al., 1989; Thompson et al., 1997). The deposited

* Corresponding author.
E-mail addresses: mona.stockhecke@eawag.ch (M. Stockhecke), flavio.anselmetti@eawag.ch (F.S. Anselmetti), feraygokdere@yyu.edu.tr (A.F. Meydan), daniel.odermatt@geo.uzh.ch (D. Odermatt), sturm@eawag.ch (M. Sturm).

0031-0182/$ – see front matter © 2012 Elsevier B.V. All rights reserved.
doi:10.1016/j.palaeo.2012.03.022

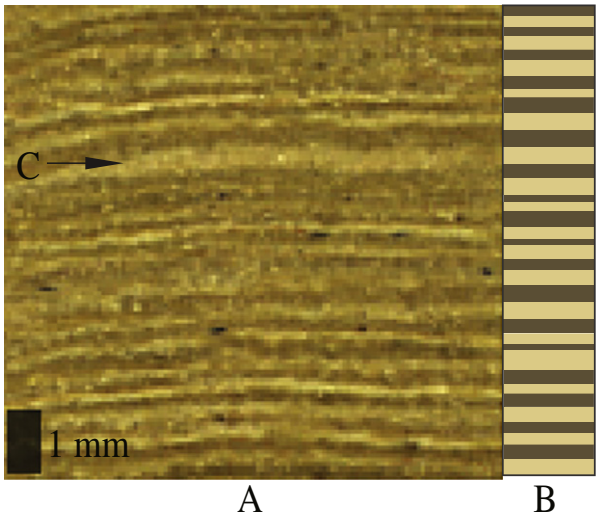

Fig. 1. The biogenic–chemical varves of Lake Van comprise couplets of light and dark laminae. (A) Photograph of sediment core Van07-05 (17.5–18.3 cm; Stockhecke, 2008) from the Tatvan Basin mooring site (Fig. 2). (B) 18 light–dark couplets (i.e., varve years) are identified, which give an averaged sedimentation rate of 0.44 mm year^{-1}. (C) The thickness of the lamina varies annually; the arrow points to an exceptionally thick light lamina.

carbonates are the source of several proxies that can be used in paleoenvironmental investigations; e.g., total inorganic carbon (TIC), the Mg/Ca ratio, and $\delta^{18}O$ (Lemcke and Sturm, 1997).

Here we report the results of monitoring seasonal and interannual particle dynamics in Lake Van from July 2006 to August 2009. Well-established limnological methods involving water-column measurements and sequential sediment traps, supplemented with state-of-the-art remote-sensing methods, are used to define the annual particle cycle and to determine the nature and timing of the processes responsible for sediment formation in Lake Van. Multiple techniques are employed to provide a micro-scale characterization of the particles, to describe their appearance, and to quantify the seasonal fluxes of inorganic and organic material. In addition, the annual particle cycle is related to the meteorological conditions in the Lake Van area.

2. Study site

Lake Van (Fig. 2) is the world's fourth-largest hydrologically closed lake by volume, and the world's largest soda lake by area (volume 607 km^3, area 3570 km^2, maximum depth 460 m, pH ~9.7, salinity ~21 g kg^{-1}; Kempe et al., 1991; Kaden et al., 2010). It is situated on a high plateau in eastern Anatolia, Turkey, at an altitude of 1648 m above sea level (a.s.l.). Lake Van fills the eastern part of a tectonic depression that was closed in the Upper Pliocene, probably because of volcanic activity (Sengör et al., 1986). The eastern part of the lake is characterized by a shallow lacustrine shelf, while the central Tatvan Basin, a deep, quasi-circular plane, occupies 440 km² and has an average depth of 445 m (Degens and Kurtmann, 1978). An elongated sedimentary ridge (the Ahlat Ridge) at the northern edge of Tatvan Basin lies at ~350 m water depth. The catchment area of 12,500 km^2 (Kadioğlu et al., 1997) is divided into three zones: a southern part consisting primarily of metamorphic rocks of the Bitlis Potruge Massif; an eastern part comprising Tertiary and Quaternary conglomerates, carbonates, and sandstones; and a north-western part containing volcanic deposits (Degens and Kurtmann, 1978; Lemcke, 1996).

The climate of southeastern Anatolia, including the Lake Van area, is strongly influenced by changes in the positions of the westerly jet stream, the extension of the subtropical high-pressure belt, and the Siberian high-pressure area, which determine the boundary between humid Mediterranean and continental climate (Roberts and Wright, 1993). The local climate of the Lake Van area is characterized by strong seasonality, expressed as cold winters from December to February with mean temperatures below 0 °C, and warm, dry

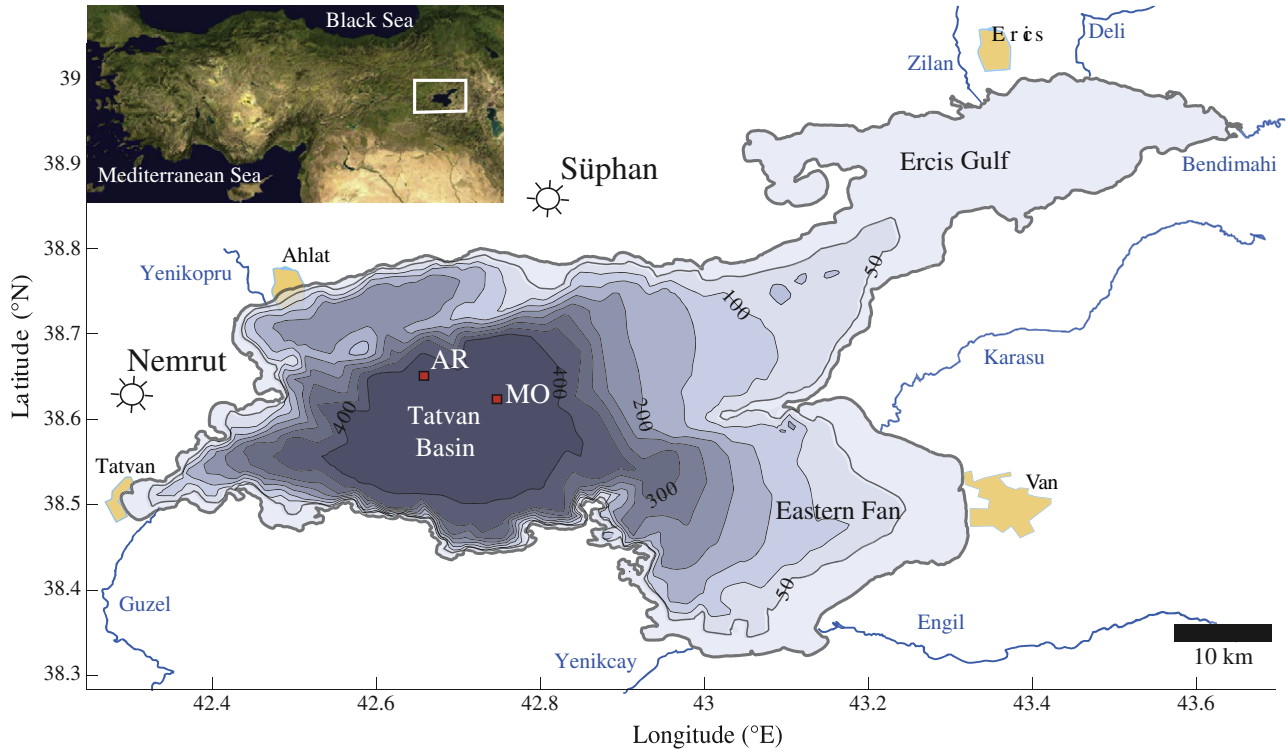

Fig. 2. Bathymetric map of Lake Van, showing the Tatvan Basin mooring site (MO), Ahlat Ridge drilling site (AR), major lake basins, river inflows and settlements. Depth contours are in meters. The volcanoes Nemrut (to the W) and Süphan (to the N) are located close to the lake.

summers in July and August with mean temperatures exceeding 20 °C. Cold, dry air masses originating from high northern latitudes acquire moisture on passing over the Mediterranean Sea, reaching Lake Van from the south-west. These south-westerly winds cause precipitation during autumn, winter and spring, whereas in summer, continental air masses originating from low latitudes result in dry conditions (Roberts and Wright, 1993).

As Lake Van is hydrologically closed, its lake level and water chemistry respond immediately to weather and climate fluctuations. The annual succession of precipitation, snowmelt, and evaporation causes seasonal lake-level fluctuations of between 50 and 90 cm (Degens and Kurtmann, 1978; Kaden et al., 2010). Lake level usually increases from January until June, when it peaks, and then decreases until December (Kadioğlu et al., 1997). Several rivers flow into the lake. Of these, the Bendimahi, Zilan and Engil rivers are responsible for 50% of the annual discharge into the lake (Fig. 2; Kempe, 1977; Reimer et al., 2008).

Lake Van's water is a brine as a result of evaporation processes, large-scale postvolcanic CO_2 activity, and hydrothermal activity (Degens and Kurtmann, 1978). Concentrations of carbonate species in the lake are about 65 times higher than in seawater, and are balanced overwhelmingly by sodium (~345 m mol L^{-1}) and potassium (~10 m mol L^{-1}). Magnesium concentrations are low (~4.5 m mol L^{-1}) and the lake is very depleted in calcium (0.087–0.105 m mol L^{-1}; Reimer et al., 2008). Salinity increases with depth, while calcium has its maximum concentration in the epilimnion (0.105 m mol L^{-1}; Reimer et al., 2008). As a result, the lake water is highly sensitive to carbonate precipitation.

3. Methods

3.1. Remote sensing

The medium-resolution imaging spectrometer (MERIS) for passive optical remote sensing, which is mounted on board the environmental satellite (ENVISAT), fulfills the requirements for mapping suspended particles in Lake Van (3-day resolution, 15 spectral bands, 300 m ground resolution). The Improved Contrast between Ocean and Land processor (ICOL; Santer and Zagolski, 2009) and the standard Case-2-Regional processor (C2R; Doerffer and Schiller, 2008) were applied to 40 MERIS full-resolution Level 1 datasets in succession. ICOL corrects for Rayleigh and aerosol adjacency effects from adjacent land surfaces (Santer and Zagolski, 2009). C2R applies an atmospheric correction and uses an inversion technique for the retrieval of water-leaving reflectances, concentrations of total suspended matter (TSM), chlorophyll-*a* (chl-*a*) and yellow substances, as well as corresponding parameters such as Z_{90}, the wavelength-dependent depth of a water column from which 90% of the reflected light originates (Doerffer and Schiller, 2008). Neither algorithm requires any parameters other than those retrieved from the input image, which is convenient for large data quantities, although it may not account for regional variations in specific inherent optical properties. Extensive application and validation campaigns document acceptable accuracies for TSM concentrations (Ruiz-Verdú et al., 2008). ICOL and C2R are freely accessible and usable without a license.

As no continuous water-quality monitoring is conducted in Lake Van, 19 water samples of 5 L each were collected at ~50 cm water depth on 27 August 2009 and on 01 July 2010. The sample locations lie along an E–W transect through the northern part of the Tatvan Basin and along a NW–SE transect through the Eastern Fan (Fig. 2). All samples were taken at least 3 km from the shore. TSM concentrations were gravimetrically determined by filtering the water samples through previously washed, dried and weighed Whatmann GF-F filters according to standard protocols (Environmental Protection Agency, 1971). Deionized water was passed through the filters to avoid bias from salt retention. Possible salt retention as described by Stavn et al. (2009) was not corrected for, as scanning electron microscopy (SEM) and energy dispersive x-ray spectroscopy (EDX) analyses of the filters did not indicate significant Cl intensities or any crystals related to lake salt. The filters were dried, weighed and normalized by sample volume. To match up the TSM concentrations determined in the laboratory (TSM_{lab}) with the corresponding remotely sensed TSM concentrations (TSM_{rs}), we extracted single-pixel TSM concentrations from the geolocated C2R outputs according to the campaign navigation data.

3.2. Conductivity, temperature, depth (CTD) measurements

Pressure (depth), temperature, turbidity, and oxygen concentration were measured with a Sea&Sun CTD60M probe (resolution and accuracy: 0.002 kPa and ±0.1 kPa for pressure, 0.001 °C and ±0.01 °C for temperature, 0.1% and ±2% for oxygen saturation, 0.1% and ±1% for light transmission). Downward profiles were measured concurrently with the water sampling on 27 August 2009 at the mooring site (MO, Fig. 2) and on 28 August 2009 in Tatvan Basin. Because calibration of oxygen saturation by Winkler titration could not be performed, only the relative changes in oxygen concentration within each profile are interpreted.

3.3. Sediment-trap sampling and temperature logging

A mooring comprising sequencing sediment traps (S-traps), integrating sediment traps (I-traps), and thermistors was installed in July 2006 in Tatvan Basin at a water depth of 445 m (38.637° N, 42.762° E; Fig. 2). The S-traps (Technicap-PPS4-3) have an active area of 500 cm^2 above a funnel-shaped inlet. A microprocessor-controlled step-motor drives a carousel of 12 cups, which automatically rotates to open each cup in turn approximately once per month. S-traps are used to measure monthly fluxes. The I-traps (Eawag-130) have two collecting cylinders with an active area of 130 cm^2 in total and an aspect ratio of 8, which ensures that no settled material is resuspended from the bottom of the trap. Total mass fluxes determined using the I-traps were used to cross-check the sequential mass fluxes measured by the S-traps and to compare trap mass fluxes with sediment accumulation rates calculated from dated sediment cores. Two types of thermistors (Vemco Minilog, with a resolution of 0.1 °C and an accuracy of ±0.2 °C; and RBR TR-1050, with a resolution of 0.0004 °C and an accuracy of ±0.002 °C) recorded the water temperature at various depths.

The mooring was deployed for the first time in July 2006. It was recovered and deployed again in September 2007, September 2008, and August 2009. For operational reasons the number of S-traps and I-traps varied from year to year. Some gaps occur between the time of closing of the last cup of the S-trap and the redeployment of the mooring. The depths and times of trapping are summarized in Table 1.

After recovery of the mooring, the sampling cups were stored at 4 °C for 48 h to ensure that all suspended particles had settled. The supernatant water was decanted for chemical analysis and checked for dissolution within the sampling cups. To remove residual saline lake water, the samples from 2007 to 2008 and 2008 to 2009 were rinsed several times until the decanted water had a pH of 7. Subsequently, the samples were freeze-dried and the total dry-weight was determined. The samples from 2006 to 2007 were freeze-dried directly and the sample mass was reduced by the amount of salt in the supernatant water to determine the mass fluxes.

The homogenized samples were analyzed for total carbon (TC) and total nitrogen (TN) using an elemental analyzer (HEKAtech Euro EA). Total inorganic carbon (TIC) content was determined using a titration coulometer (Coulometric Inc., 5011 CO2-Coulometer). $CaCO_3$ content was calculated stoichiometrically by multiplying the TIC by 8.33, assuming that all inorganic carbon is bound as calcium carbonate.

Table 1
Results of sediment trap samples and sediment core sample (0–2 cm; Stockhecke, 2008) from the Tatvan Basin mooring site. Listed are the deployment dates; type of trap (I = integrating trap; S = sequential trap); sampling interval (accumulated intervals of S-traps given in parentheses); water depth; the fluxes of total mass, $CaCO_3$, TOC, TN, and bSi; C/N ratios; and the cumulative percentages of DM, $CaCO_3$, OM, and bSi.

Deployment dates	Type	Interval	Depth	Mass	$CaCO_3$	TOC	TN	bSi	C/N	DM	$CaCO_3$	OM	bSi
		(days)	(m)	(mg m^{-2} day^{-1})					(−)	%	%	%	%
14 Jul 06–22 Jul 07	I	373	35	243	82	6	0.8	6	9	59	34	5	2
	I	373	440	298	103	8	1.0	9	9	57	35	6	3
20 Jul 06–16 Jul 07	S	18–35 (361)	440	389	131	10	1.8	12	9	58	34	6	3
26 Sep 07–07 Jul 08	S	15–35 (285)	35	401	176	12	1.9	20	8	45	44	6	5
	S	15–35 (285)	430	463	234	14	1.7	7	9	42	51	6	2
08 Sep 08–26 Aug 09	I	352	100	674	143	24	3.1	13	9	69	21	8	2
	I	352	440	433	101	18	2.3	4	9	67	23	9	1
08 Sep 08–05 Jul 09	S	15–50 (300)	440	322	73	14	1.8	7	9	66	23	9	2
Sediment core										55	35	9	1

Biogenic silica (bSi) concentrations were measured using a wet chemical digestion technique combined with ICP-AES (Ohlendorf and Sturm, 2008). Total organic carbon (TOC) was calculated as TOC = TC − TIC, and organic matter (OM) as OM = 2 × TOC + TN (Meyers and Teranes, 2001). Detrital mineral mass (DM) was quantified by subtracting $CaCO_3$ + OM + bSi from the total particle mass. Single-particle analyses were performed by scanning electron microscopy (SEM) and energy dispersive x-ray spectroscopy (EDX) using a specific spraying technique for the targets (Bollmann et al., 1999) to ensure representative subsampling of the trap material.

3.4. Meteorological and lake-level data

Precipitation and air temperature data were available from the meteorological station in Van (Fig. 2) from 1975 to 2009. Long winter (December to March) Ponta Delgada-Reykjavik (PD-R) North Atlantic Oscillation indices (NAOIs) were obtained from http://www.cgd.ucar.edu/cas/jhurrell/nao.stat.winter.html. Lake levels were available from the Tatvan discharge measurement station.

4. Results

4.1. Ground validation of MERIS data

Fig. 3 shows the highly variable TSM_{lab} and TSM_{rs} concentrations in the surface waters. The 19 match-ups of TSM_{lab} and TSM_{rs} concentrations show that the ICOL and C2R algorithms perform well at concentrations above 1 mg L^{-1} (measured mostly in 2010), which correspond to the occurrence of whitings, but much less well at concentrations below 1 mg L^{-1} (measured mostly in 2009). The sensitivity for $TSM_{lab} > 1$ mg L^{-1} ($dTSM_{rs}/dTSM_{lab} = 1.38$) substantially exceeds that for $TSM_{lab} \leq 1$ mg L^{-1} ($dTSM_{rs}/dTSM_{lab} = 0.15$).

At all nine of the sites sampled during 2009, the maximum turbidity was found at ~25 m water depth. However, Z_{90} as calculated by the C2R algorithm is 15 m for the eight low-TSM_{rs} locations and 8 m for the one high-TSM_{rs} location.

Significant spectral differences between high-TSM_{rs} and low-TSM_{rs} pixels were observed. At high-TSM_{rs} locations (i.e., within whitings), the visible wavelength reflectances were about twice as high as at low-TSM_{rs} locations. In addition, the spectra of the visible-wavelength reflectances showed a sharp increase from 442.5 to 490 nm at high-TSM_{rs} locations, but remained flat at low-TSM_{rs} locations. $CaCO_3$ particles have higher refractive indices and scatter light more than other mineral species with an identical concentration and size distribution (Stramski et al., 2007). Dierssen et al. (2009) described overall elevated reflectances with a peak at 490 nm for whiting events in the Bahamas, which is consistent with the ICOL-C2R-processed MERIS data from whitings in Lake Van.

4.2. Time-series of true color composites and TSM images

A series of nine image pairs taken between August 2006 and July 2007 (Fig. 4) shows how water color, TSM_{rs} concentration, and catchment snow-cover changed during this time period. Distinct changes in water color with sharp boundaries are visible in the true-color composite image of Lake Van, indicating different water masses. The turbid waters are brighter because of higher backscattering by the suspended particles. Dark water masses indicate predominantly absorbing water with lower particle scattering. These different water colors, or different degrees of turbidity, carry significant information about the lake's surface current system. A prominent turbidity decrease from east to west and from the lake shore to the center of the lake, as well as surface currents, is visible in all nine image pairs. In the deep areas (Tatvan Basin), counterclockwise eddies with a clear center surrounded by turbid water are apparent (Fig. 4). In shallow or narrow areas such as Ercis Gulf and the Eastern Fan, clockwise currents can be seen (Fig. 2).

Water color and TSM_{rs} concentrations varied greatly during the 12 months from August 2006 to July 2007 (Fig. 4). In August 2006 (Fig. 4A) and September 2006 (Fig. 4B) the lake was dark blue with distinct, white, cloudy patterns corresponding to areas of enhanced

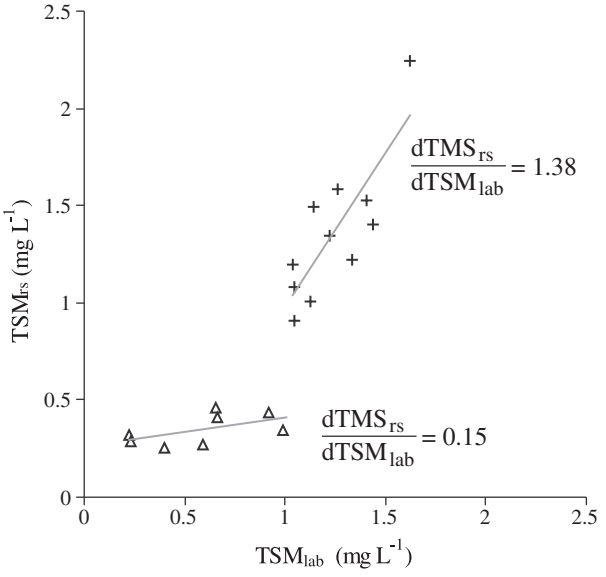

Fig. 3. Relationship between total suspended matter concentrations determined using the ICOL and C2R algorithms (TSM_{rs}) and those determined by the filtration of water samples in the laboratory (TSM_{lab}). The relationship can be described in terms of two linear regressions, one for high-TSM concentrations (triangles, $TSM_{lab} > 1$ mg L^{-1}: $n = 11$, $r^2 = 0.67$, $p < 0.1$) and one for low-TSM concentrations (crosses, $TSM_{lab} \leq 1$ mg L^{-1}: $n = 8$, $r^2 = 0.32$, $p < 0.05$).

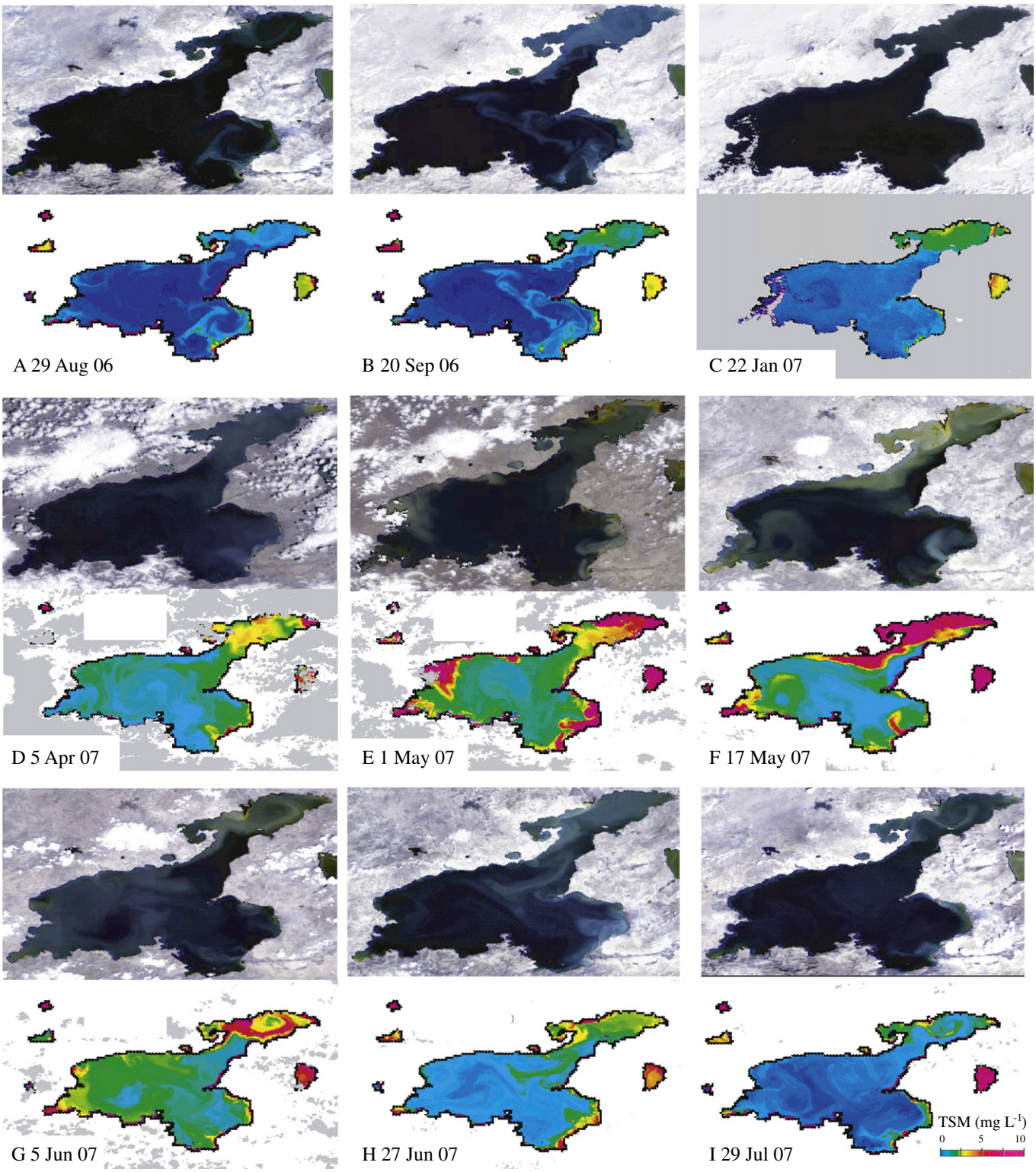

Fig. 4. Time-series of MERIS image pairs of Lake Van, each with true-color composites above and a TSM_{rs} concentration map below. Areas in gray in the TSM_{rs} concentration maps are pixels where the algorithm set the "bright" flag to indicate clouds or snow (specific threshold at 442.5 nm).

TSM_{rs} concentration that covered a total area of 50 to 100 km^2. Maximum reflectances of the bright pixels occurred around 490 nm. In January 2007 (Fig. 4C), when the catchment was completely covered with snow, these patterns disappeared. In April and May 2007 (Figs. 4D–F) the snow melted and brownish surface plumes of high TSM_{rs} concentration were formed close to the river inlets in Ercis Gulf, south of the city of Van, and near the central part of Tatvan Basin. The brownish surface plumes had their maximum reflectances around 560 nm. They were less prominent in Ercis Gulf at the beginning of June 2007 (Fig. 4G) than two weeks earlier, although TSM_{rs} concentrations remained high. Surface-water clouds of carbonate precipitation (whitings) appeared over the whole surface of Tatvan Basin, and extended even as far as the northern part of the lake throughout June and July (Figs. 4H, I).

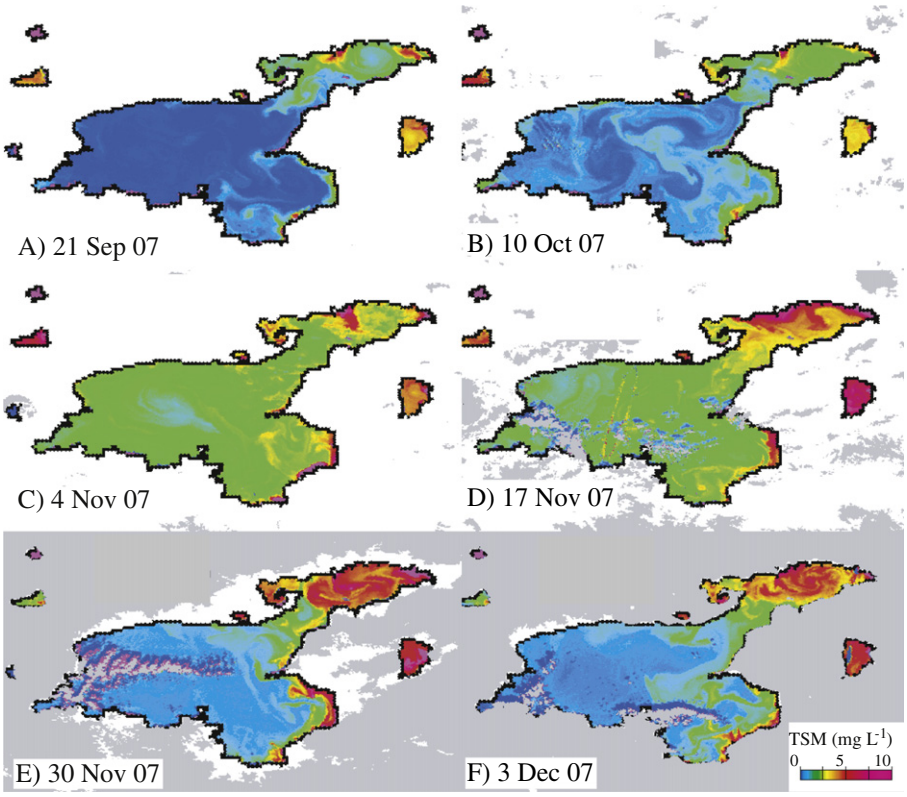

Fig. 5. Time-series of six maps of Lake Van showing TSM_{rs} concentrations. The acquisition dates are indicated by arrows in Fig. 9. Areas in gray are pixels where the algorithm set the "bright" flag to indicate clouds or snow (specific threshold at 442.5 nm).

A second series of six images from the fall and early winter of 2007 (Fig. 5) reveals an exceptional event of high-particle concentrations. TSM_{rs} concentrations on 21 September 2007 (Fig. 5A) and 10 October 2007 (Fig. 5B) were close to zero in Tatvan Basin, but during October and November they increased throughout the lake (Figs. 5C, D). The last two images from 30 November 2007 (Fig. 5E) and 03 December 2007 (Fig. 5F) indicate that TSM_{rs} concentrations had declined once again in the Tatvan Basin but remained high in the Ercis Basin.

4.3. Water-column properties

The temperature profile taken in Tatvan Basin on 28 August 2009 (Fig. 6) shows a temperature decrease with depth from 21.5 °C at the water surface to 3.3 °C in the hypolimnion. The turbidity profile shows a 25-m-thick layer of particulate matter in the metalimnion at 15 to 40 m water depth, with a maximum at 26 m water depth. The oxygen concentration increased with depth to reach a maximum at 30 m. The 4-m depth difference between these maxima is likely to be an artifact resulting from the response time of the oxygen sensor (10 to 30 s) of the CTD equipment, which was lowered at ~0.3 m s^{-1}. Below 30 m, the oxygen concentration decreased with depth, and at ~250 m water depth, a drop in oxygen concentration, combined with a rise in turbidity, may indicate the precipitation of iron and manganese minerals (Kaden et al., 2010), which can be interpreted as a transition from oxic to anoxic water conditions. As above, a vertical shift between the oxygen and turbidity measurements is presumably an artifact related to the slow response time of the oxygen probe. The traces of oxygen (0.4 mg L^{-1}) recorded below 250 m are a result of the limited accuracy of the sensor, but anoxia at this depth can be assumed, as the water smelled strongly of H_2S and no brown manganese precipitates were formed in the deep-water sample after fixation with manganese sulfate.

The interpolated temperatures within the upper 70 m from July 2006 to March 2008 show that the lake was stratified from May to November (Fig. 7). A ~10 m thick epilimnion with temperatures of up to 25 °C developed in May after winter mixing and remained until late fall. In fall 2007, mixing occurred two weeks later than in 2006. Water-column mixing affected the entire upper 70 m until January, generating a homogeneously cold water column at 3.4 °C until at least March. Below 70 m the water temperature ranged from 3.2 °C to 3.7 °C.

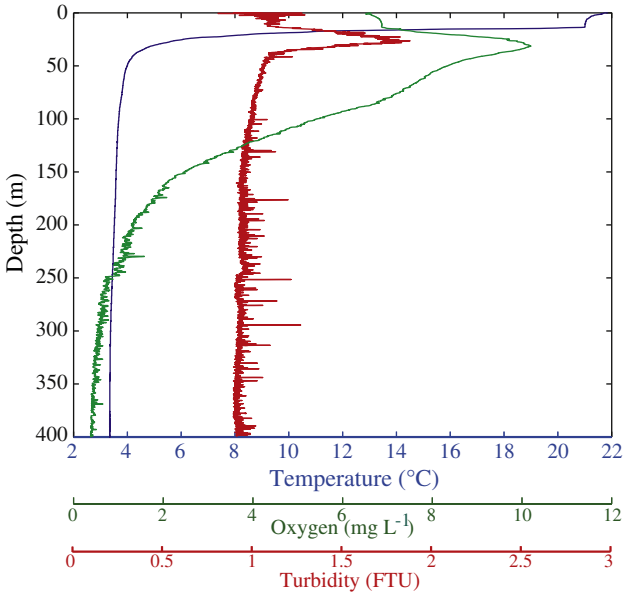

Fig. 6. Temperature, turbidity (in Formazin Turbidity Units), and oxygen profiles acquired with a CTD probe at the Tatvan Basin mooring site on 28 August 2009.

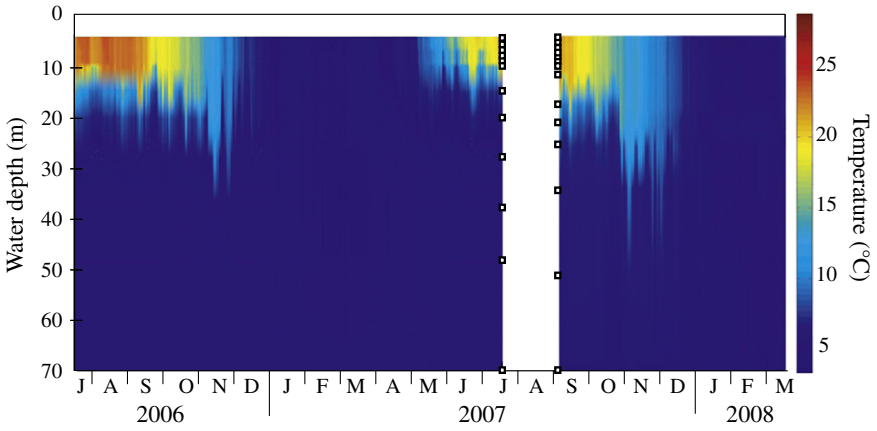

Fig. 7. Interpolated water temperatures (°C) in the uppermost 70 m of Lake Van from July 2006 to July 2007 and from September 2007 to January 2008. The thermistors were deployed at the depths indicated by squares during each of the two periods.

4.4. Particle characterization and composition

Four different particle groups were found in the sediment-trap samples (Fig. 8): (1) autochthonous calcite crystals ($CaCO_3$); (2) non-silicified organic material (OM); (3) biogenic silica (bSi); and (4) detrital minerals (DM). They were appeared as single particles, as amorphous aggregates (sticking together by coagulation), or as fecal pellets. The fecal pellets (10 to 60 μm in length) consisted of a mixture of calcite crystals and silicified frustules (Figs. 8A, C). The calcite crystals were <1 to 10 μm long (Fig. 8B). Calcite crystals with surfaces etched by dissolution were found in the spring samples. In the June 2007 samples, almost no single calcite crystals occurred, but SEM EDX analysis showed high Ca intensities in all particle aggregates. In the fall samples, the calcite crystals were even smaller than in the spring samples, and showed a complex structure. Silicified frustules comprised of pennate and centric diatoms of various sizes, as well as chrysophycean cysts, were found in all samples, and were especially abundant in fall 2007 (Fig. 8C–F). No significant amounts of terrestrial plant remains were found. In all trap samples, C/N ratios were ~9 (Table 1).

The mean total mass flux, based on all S-trap and I-trap samples, was 403 mg m^{-2} day^{-1}. This comprised 33% $CaCO_3$ (with up to 67% in individual samples), 7% OM, 3% bSi and 58% DM (Table 1). The compositions of the I-trap and mean S-trap samples from each year were consistent regardless of deployment depth and trap type, and compare well with the composition of the surface sediment. The organic components (OM and bSi) accounted for ~10% of the total in each of the three years. $CaCO_3$ and DM fluctuated by up to 23% from one year to the next. The fluxes in the deep I-trap are higher than those in the shallow trap, except for the sampling period September 2008 to August 2009 (Table 1). The mean total mass flux of 403 mg m^{-2} day^{-1} in Tatvan Basin is consistent with the

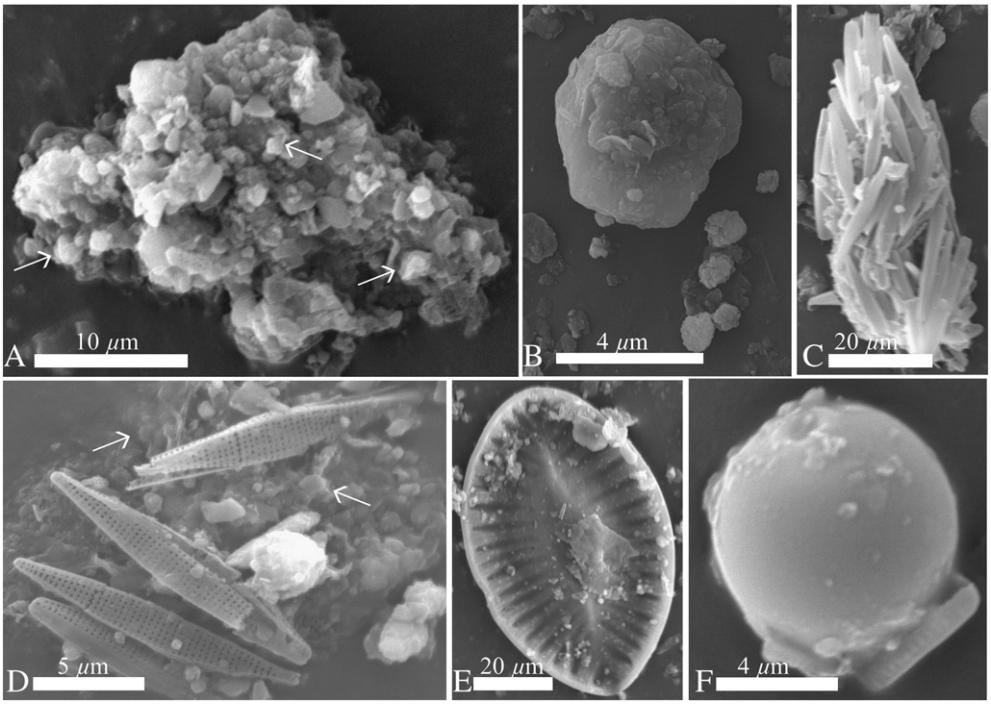

Fig. 8. Scanning electron microscope images of sediment-trap samples taken in spring, summer, and fall from 440 m water depth in Lake Van. (A) Calcareous particle aggregates; the arrows point to calcite crystals (S-trap sample, 08 March–12 April 2007). (B) Autochthonous calcite crystals (S-trap sample, 27 March–16 April 2008). (C) Fecal pellet consisting of pennate diatoms (S-Trap sample, 08 March–12 April 2007). (D) Pennate diatoms; the arrows point to calcite crystals (I-trap sample, 14 July 2006–22 July 2007). (E) Pennate diatom (S-trap sample, 08 March–12 April 2007). (F) Chrysophycean cyst (S-trap sample, 14 September–19 October 2006).

sediment accumulation rate of 500 mg m^{-2} day^{-1} determined by Lemcke (1996) from dated Holocene sediment cores.

4.5. Sequential trap fluxes of total mass, $CaCO_3$, DM, TOC, and bSi

Fig. 9 depicts the fluxes of total mass, $CaCO_3$, DM, TOC, and bSi measured in the 36 deep trap samples (440 m, red solid line) between July 2006 and June 2009, and in the 12 shallow trap samples (35 m, green dotted line) between September 2007 and July 2008. The total mass fluxes calculated from the deep trap vary from almost zero to 1297 mg m^{-2} day^{-1} (Fig. 9A). Seven periods of high mass flux were recorded: three in spring, three in fall and one in summer (Fig. 9A (1)–(7)). These periods were interrupted by periods of low flux during winter and by sampling gaps during July and August, except for the early summer of 2007. Except for period (5), the periods of high mass flux reflect $CaCO_3$ pulses that occurred simultaneously with the high fluxes of DM, TOC, and bSi. The bSi data show periods of high flux less markedly than the data of the other proxies, with the exception of the bSi peaks in October 2006 (in 440 m) and May 2008 (in 35 m) (Fig. 9E). The bSi fluxes measured in fall 2006

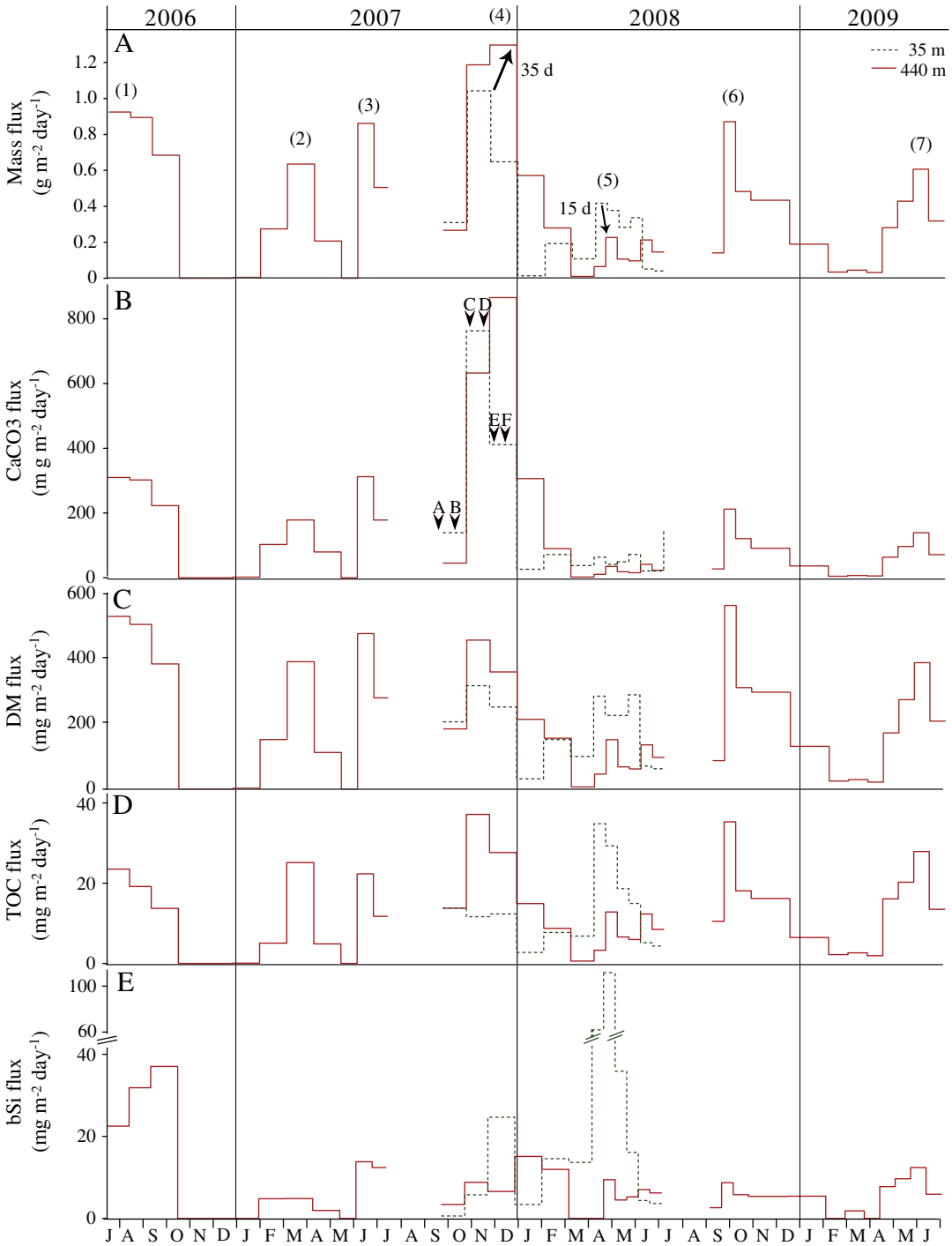

Fig. 9. Time-series of Lake Van S-trap data from the metalimnion at 35 m depth (green dotted line) and the hypolimnion at 440 m depth (red solid line). (A) Total mass flux. (B) $CaCO_3$ flux. (C) DM flux. (D) TOC flux. (E) bSi flux. In A, numbers (1) to (7) indicate periods of high mass fluxes and black arrows indicate delay times of 35 and 15 days between the arrival of particle flux peaks at 35 and 440 m depth. In B, the arrows and letters (A to F) mark the acquisition dates of the satellite images shown in Fig. 5.

and fall 2007 in the deep trap peaked one sampling interval after the TOC flux. A comparison of the times of occurrence of the peaks in total mass flux at the shallow and deep traps reveal that the maximum time taken for the particles to settle between the two traps was ~70 days in 2007 and ~30 days in 2008; however, effective settling times may be shorter. With regard to temporal variability, flux magnitudes and composition, the pattern in 2007–2008 is different from the patterns in 2006–2007 and 2008–2009 (Fig. 9, Table 1). The main differences between the period 2007–2008 and the preceding period are (1) the occurrence of a $CaCO_3$ peak during a time when no significant $CaCO_3$ precipitation would have been expected (26 October to 30 December 2007); and (2) an intermediate mass flux in April 2008, characterized by high fluxes of TOC and bSi and low $CaCO_3$ fluxes.

4.6. Meteorological conditions

Based on the available meteorological data from Van (1975–2009), the monthly total precipitation (maximum 53 mm, minimum 4 mm; annual sum 379 mm) and monthly mean air temperatures (maximum 22.4 °C, minimum −3.3 °C; annual mean 9.3 °C) reflect the continental climate of eastern Anatolia, with its pronounced seasonality and high annual variability in precipitation and temperature (black lines in Fig. 10). Interannual variability was assessed by calculating the deviation of the monthly precipitation and temperature values from July 2006 to June 2009 from the 1975–2009 mean values in Van (bars in Fig. 10). These precipitation and temperature anomalies (bars in Fig. 10) thus represent the departure from the long-term mean and large anomalies are considered as 'unusual' conditions. Positive anomalies indicate wetter (warmer) conditions, while negative anomalies indicate drier (cooler) conditions.

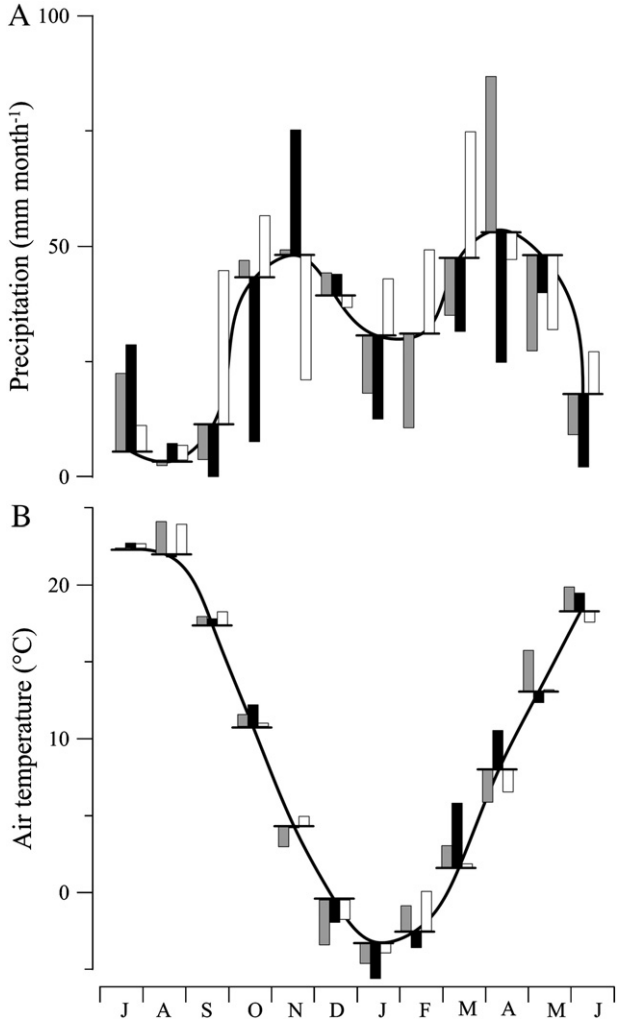

Fig. 10. (A) Monthly total precipitation and (B) monthly mean air temperature from July to June in Van (see Fig. 2 for location). Monthly means based on 35 years of data (1975–2009; black lines) show a typically continental annual pattern. The precipitation and temperature anomalies illustrated in gray (2006–2007), black (2007–2008), and white (2008–2009) represent the interannual variability during the study period.

The total annual precipitation in Van was 356 mm from July 2006 to June 2007, 304 mm from July 2007 to June 2008, and 450 mm from July 2008 to June 2009. In fall, precipitation is usually high in October and November, while September is dry (black line in Fig. 10A). Monthly mean air temperatures decrease from September to December, with October temperatures lying above 0 °C and only a few frost days in November (black line in Fig. 10B). Temperatures below 0 °C persist in December, when precipitation is stored in the catchment as snow. Mean lake level increased from 1649.02 m a.s.l. in 2006–2007 to 1649.47 m a.s.l. in 2007–2008, but remained stable at 1649.42 m a.s.l. in 2008–2009. Monthly precipitation anomalies during the study period were generally high, ranging from −36 to 34 mm $month^{-1}$ with an annual mean of 14 mm $month^{-1}$. On an annual scale, the highest monthly precipitation anomalies persisted during the relatively dry periods of 2007–2008 (annual mean 16 mm) and 2006–2007 (12 mm). The monthly precipitation anomaly during the relatively wet year 2008–2009 was slightly lower than during 2007–2008 (15 mm). During the measurement period, the temperature anomalies were low (mean 1.3 °C) with a tendency toward negative anomalies during winter and positive anomalies during spring, summer and fall (Fig. 10). The long winter (December–March) PD-R NAOIs were positive throughout the sampling period (1.5 in 2006–2007, 1.1 in 2007–2008, and 0.7 in 2008–2009), but the PD-R NAOI was negative in November 2007 (−1.2).

5. Discussion

5.1. Spatial hydrological and sedimentological processes

The turbidity profile in August 2009 showed maximum particle concentrations occurring between 15 and 40 m water depth, at water temperatures between 5 °C and 15 °C, coinciding with an oxygen maximum (Fig. 6). This suggests that at least part of the turbidity signal is related to primary productivity. Decreasing turbidity and oxygen values below 26 m and 30 m, respectively, indicate that these depths represent the lower boundary of the photic zone. Below the photic zone, particles settle and dead organic material degrades, resulting in oxygen uptake. The nature of the non-uniform vertical particle distribution and the fact that the turbidity maximum in the profile occurs at a greater depth (~26 m) than the depth determined by remote sensing (8 to 15 m) indicate that TSM concentrations in the upper 40 m of the water column would always be significantly higher than those determined by remote sensing. The validation campaign showed that the algorithm performs well for concentrations above 1 mg L^{-1} and represents the TSM concentrations down to about 8 to 15 m water depth.

The vertical particle distribution, as measured in the turbidity profile, explains the differences in the mass fluxes sampled with the I-traps at different depths (Table 1). In the period 2008–2009, the shallow trap was installed at 100 m water depth — i.e., 64 m below the photic zone and under oxygen-rich conditions. In the two previous periods, however, the shallow trap had been installed at 35 m water depth, within the metalimnion and at the lower boundary of the photic zone, and thus probably did not collect the particles from the entire productive zone. The two sets of S-trap samples in 2007–2008 showed that the time taken for particles to settle from 35 to 440 m was substantially less than one season (3 months).

Thus the data from the deep trap are able to capture the seasonal fluctuations in epilimnetic particle formation even when the lake is stratified. However, the particles are altered in two ways during sinking. First, the different particle components are aggregated as a result of water-filtering organisms, such as the halophilic crustacean *Artemia*. Fecal pellets of similar size and structure produced by *Artemia* have been described for saline Lake Urmia in Iran (Kelts and Shahrabi, 1986). Second, the silicified frustules and calcite crystals are partly dissolved. Silicified frustules respond most sensitively to nutrient concentrations, salinity and high pH values, especially within the epilimnion, where temperatures are high (Honjo, 1996). However, many entire frustules were preserved within the sediment traps. Also, the composition of the trap samples within each year was consistent. We conclude therefore that the trap samples were not affected significantly by dissolution, resuspension or any other disturbances, and that the S-trap samples represent the vertical particle fluxes at seasonal resolution.

The upper boundary of the anoxic zone rose from ~440 m in 1990 to 325 m water depth in 2005 (Kaden et al., 2010). This trend continued at least until 2009, when it rose to 250 m. This implies that the water column of Lake Van did not undergo complete mixing during the entire period from 1990 to 2009.

The qualitative to semi-quantitative observations based on true color composites and TSM_{rs} estimates are capable of giving new insights into the lateral dynamics of particle-relevant processes that complement those derived from the mooring data. The observed lateral turbidity decrease from east to west appears to follow the general bathymetry of the lake basin (Fig. 2). However, a systematic bathymetric influence is unlikely, because the detailed pattern shown by each of the images is different, and because on average, at ~2 km distance from the shore, water depths already exceed 50 m. The locations of the turbidity plumes correspond to the three main inflowing rivers: the Bendimahi, Zilan and Engil (Fig. 2). Thus, the eastward turbidity increase results from the inflow of fresh river water that overlies the denser saline lake water. The inflow carries detrital minerals and supplies dissolved Ca^{2+} ions, leading subsequently to carbonate precipitation. The brownish turbidity plumes in the lake near the mouths of the rivers are interpreted as resulting mainly from fluvially transported detrital particles. The almost white turbidity plumes are interpreted as whitings. Interflows and underflows are not expected to occur because of the high density of the saline lake water (Kaden et al., 2010). Therefore, because turbidity decreases significantly in the surface waters towards the lake center, a significant part of the fluvially transported detrital material must be deposited in the Ercis Gulf, while at the mooring position, eolian material must be proportionally greater (compared to the Ercis Gulf). The satellite images provide further documentation of the basin-wide occurrence of carbonate precipitation and whitings at the mooring site (Fig. 4).

5.2. Seasonal pattern of particle fluxes

The particle-mass flux follows an annual cycle, with high values occurring between spring and fall, and low values during winter (Fig. 9). This is confirmed by the satellite images, which also indicate the existence of medium to high particle fluxes during summer (Fig. 4). Most of the variability in particle-mass flux is controlled by the usual pattern of climate conditions (black lines in Fig. 10). The precipitation and air temperature patterns result in a high runoff in spring (precipitation and snow-melt) and late fall (precipitation increase before the onset of freezing temperatures), and low runoff in summer and winter. The runoff delivers dissolved Ca^{2+} ions and detrital material to the lake, where they trigger calcite precipitation. The $CaCO_3$ pulses occur simultaneously with the trapping of silicified or non-silicified algae, and coincide with the turbidity and oxygen maxima within the water column (Fig. 6). This pattern suggests that photosynthetic CO_2 removal and the availability of cells as nucleation sites (Sturm et al., 1982; Stabel, 1986; Thompson et al., 1997) also contribute to the precipitation of carbonates. As the annual lake level fluctuates independently of the mass fluxes (decrease of ~60 cm from July to December) the effect of evaporative supersaturation cannot be assumed as a major control of calcite precipitation.

In spring, runoff reaches its maximum and water temperatures increase. Calcite precipitation is observed as strong lateral gradients in TSM_{rs} concentration and as turbidity plumes at the river mouths. Simultaneously, algal blooms occur in response to the increasing temperature of the nutrient-rich lake water after winter mixing. Together, these two factors explain the increasing fluxes of TOC, bSi and $CaCO_3$. Nutrient uptake and the cessation of freshwater input lead to the subsequent decrease in the fluxes of inorganic and organic particles. During summer, carbonate precipitation continues in Tatvan Basin, but not at such a high rate as in spring and autumn (Figs. 4H, I). No significant precipitation occurs, and the reduced river runoff is related to snowmelt. Lake levels decrease and the water becomes strongly stratified (Fig. 7). Carbonate precipitation during summer might be associated with high organic productivity coupled with strong stratification (Huguet et al., 2011) and evaporative supersaturation. During fall, TOC production and carbonate precipitation are slightly higher than during spring, and turbidity plumes are visible (Fig. 4B). Precipitation increases in late fall, leading to an increase in runoff, so that Ca^{2+} again enters the supersaturated water (Fig. 10). Together with the decaying stratification, this causes the second pulse of carbonate precipitation of the year. With the onset of freezing air temperatures, runoff decreases and the lake water starts to mix. Cold water temperatures and snowfall inhibit carbonate precipitation during winter. The remaining organic particles trapped at the thermocline settle out and sink through the homogeneous water column.

5.3. Interannual variability of the annual particle cycle

Interannual variations in particle flux correspond to the precipitation and air temperature anomalies. Precipitation and temperature in late fall and winter 2006 corresponded largely to the long-term patterns, but were anomalous in 2007 and 2008. The response of the mass fluxes to the precipitation and temperature anomalies was significant in late fall and winter 2007, whereas the particle cycle was 'as usual' in 2008. An anomalous $CaCO_3$ precipitation event in early winter 2007 was documented in the TSM_{rs} concentrations and $CaCO_3$ fluxes. TSM_{rs} concentrations prior to the carbonate peak were close to zero in Tatvan Basin, corresponding to a flux of 139 mg $CaCO_3$ m^{-2} day^{-1} (Fig. 5A, B). The high, area-wide TSM_{rs} concentrations in November coincided with maximum carbonate fluxes of 762 mg $CaCO_3$ m^{-2} day^{-1} (Fig. 5C, D). Subsequently, the TSM_{rs} concentration and $CaCO_3$ flux (411 mg $CaCO_3$ m^{-2} day^{-1}) decreased again (Fig. 5E, F). Negative precipitation anomalies and positive temperature anomalies were recorded during October 2007 (drier and warmer) and positive precipitation anomalies were recorded during November 2007 (wetter) (Fig. 10). The dry and warm October and the wet November led to: (1) highly supersaturated, warm surface water (associated with a decrease in lake level of ~1 m from September to October); (2) high, long-lasting November runoff (late onset of freezing temperatures, after 30 November 2007); and (3) late mixing of the water column (14 days later than in 2006; Fig. 7). Hence, the presence of highly supersaturated, warm surface water coincided with exceptionally late and high runoff, so that the $CaCO_3$ event can be linked directly to these anomalous weather conditions. The anomalous winter of 2007–2008 was followed by a spring that was characterized by anomalously dry conditions until June, which led to reduced runoff and carbonate production but did not affect the fluxes of organic matter and silicified algae. In contrast to 2007, positive precipitation anomalies were recorded during September and October

2008 (wetter) and negative precipitation anomalies were recorded during November 2008 (drier), but these anomalies apparently had no strong effect on particle formation. The interannual variability in the particle flux shows that the effects of specific air temperature and precipitation patterns occurring during some winters were recorded sensitively in the sediment traps, and, consequently, in the sedimentary succession. With the exception of November 2007, the study was conducted during a positive phase of the NAO, which implies rather cold and dry conditions in Turkey (Cullen and deMenocal, 2000).

5.4. Varve formation

The long-term strong seasonality in precipitation and temperature results in an annually repeating seasonal particle cycle, despite great interannual variability. In Lake Van, this particle cycle is recorded within a varved sediment record that is traceable throughout the entire deep zone of the lake. Varves have even been observed in water depths as shallow as 50 m in Ercis Gulf, and 100 m in the Eastern Fan area (Stockhecke, 2008).

Macroscopically, each varve can be defined as a couplet comprising one light and one dark lamina (Fig. 1). Previous studies suggested that light laminae represent deposition associated primarily with spring runoff, and secondarily with summer evaporation (Landmann et al., 1996; Lemcke, 1996; Lemcke and Sturm, 1997). It has also been stated that the light laminae are formed as a result of evaporation and mixing of Ca-rich riverine water and alkaline lake water in late summer (Landmann and Kempe, 2005). The sediment-trap time series, however, clearly imply that the light laminae typically begin to form in early spring, with deposition continuing through summer and, with increasing rates, in fall. As a consequence, the light laminae represent the combined effect of spring runoff (i.e., snowmelt and precipitation), summer productivity, fall mixing, and runoff associated with rain occurring before the onset of winter snowfall. As described by Lemcke (1996), the dark-colored laminae are deposited during winter (Fig. 1B) and represent the cold, unstratified lake state. Exceptionally thick layers can also be recognized in the sedimentary record (Fig. 1C) that might reflect exceptional weather conditions, such as winter rain as opposed to snow, as observed in late fall and early winter of 2007 (Fig. 10). These anomalous conditions trigger $CaCO_3$ precipitation events that punctuate the regular annual particle cycle. Microscopically, boundaries between the light and dark laminae are gradual, and carbonate crystals can also occur within the dark laminae. Overall, however, sediment formation is controlled by seasonal variability in the flux of $CaCO_3$ (spring–summer–fall on the one hand, and winter on the other), which eventually gives rise to the typical couplets of light and dark laminae found in the sediment of the lake.

6. Conclusions

Three years of monitoring and tracking seasonal particle pulses in Lake Van have enabled us, for the first time in this lake, to link the seasonal particle fluxes to hydrological and meteorological forcing that is ultimately controlled by atmospheric circulation patterns. The sediment-trap data were complemented by remotely-sensed total suspended-matter concentrations, validated by simultaneous water-column sampling, that show great temporal and lateral variations resulting from whitings and turbidity plumes. The water column undergoes seasonal stratification. During the period of study, mixing down to 70 m depth started in fall, but because the water column was not mixed entirely, the bottom water remained anoxic. On average, the sediment trap samples consisted of 33% autochthonous calcium carbonate, 7% aquatic organic matter (non-silicified algae), 6% biogenic opal (diatoms and chrysophycean cysts), and 54% detrital minerals. Interannually, the proportions of inorganic components fluctuated, whereas the proportions of organic components remained relatively constant. The observed mean mass flux of 403 mg m^{-2} day^{-1} corresponds well with Holocene sediment accumulation rates of 500 mg m^{-2} day^{-1} that have previously been determined in Tatvan Basin. Sequential sediment-trap data revealed that the annual particle cycle is characterized by high particle fluxes during spring and fall, medium fluxes during summer, and almost zero flux during winter. High runoff during spring (precipitation and snowmelt), high productivity during summer, and high runoff (precipitation before snowfall starts) and mixing during fall control the $CaCO_3$ fluxes. Interannual variability, such as an extraordinary high $CaCO_3$ flux in November 2007, can be linked to precipitation and temperature anomalies. The monitoring of the annual particle cycle clearly implies that the light laminae typically begin to form in early spring. Deposition continues throughout summer, and lasts with increasing deposition rates, until fall. Consequently, the light laminae represent the merged effect of spring runoff (i.e., snowmelt and precipitation), summer productivity, fall mixing, and precipitation before snowfall starts. The dark laminae, which are deposited during winter, represent the cold, unstratified lake state. Consequently, the varve succession is a direct product of seasonally changing environmental conditions, and is especially sensitive to alterations in precipitation. Hence, if different varve lithologies are encountered, different seasonal climate forcings can be postulated. The results of the modern calibration thus provide a basis for the reconstruction of past seasonal climate patterns by analyzing the varved lithologies within the sediment cores recovered in 2010 by the ICDP-Paleovan project, which cover several glacial–interglacial cycles.

Acknowledgments

We thank Rolf Kipfer and Yama Tomonaga for their special efforts during fieldwork and for helpful discussions. Heike Kaden and Frank Peeters from the University of Konstanz, Germany, are acknowledged for providing the thermistors and processing the thermistor data. Thanks go to Sefer Örcen and Mustafa Karabiyikoglu from the Yüzüncü Yıl Üniversitesi of Van, Turkey, for their cooperation and support, and to the ship's crew, Mete Orhan, Mehmet Sahin, and Münip Kanan for their strong commitment. For field and laboratory assistance we would like to thank Irene Brunner, Alois Zwyssig, and Brian Sinnet from Eawag. We gratefully acknowledge the linguistic help of David M. Livingstone. Medium resolution imaging spectrometer (MERIS) data were made available through the European Space Agency (ESA). Meteorological data were provided by the Turkish State Meteorological Service, and lake-level data by the Turkish General Directorate of Electric Power Resources Survey and Development Administration (EIE). We are grateful to the two reviewers and editor who spent time to provide constructive comments and suggestions which improved the manuscript deeply.

References

Bollmann, J., Brabec, B., Cortés, M.Y., Geisen, M., 1999. Determination of absolute coccolith abundances in deep-sea sediments by spiking with microbeads and spraying (SMS-method). Marine Micropaleontology 38, 29–38.
Brauer, A., Haug, G.H., Dulski, P., Sigman, D.M., Negendank, J.F.W., 2008. An abrupt wind shift in western Europe at the onset of the Younger Dryas cold period. Nature Geoscience 1, 520–523.
Broecker, W.S., 2002. The Glacial World According to Wally, Third Ed. Eldigo Press, New York.
Cullen, H.M., deMenocal, P.B., 2000. North Atlantic influence on Tigris–Euphrates streamflow. International Journal of Climatology 20, 853–863.
De Geer, G., 1910. A geochronology of the last 12,000 years, XI. International Geological Congress Stockholm 1910, C.R. .
Degens, E., Kurtmann, F., 1978. The Geology of Lake Van, Vol. 169. MTA Press.
Dierssen, H.M., Zimmermann, R.C., Burdige, D.J., 2009. Optics and remote sensing of Bahamian carbonate sediment whitings and potential relationship to wind-driven Langmuir circulation. Biogeosciences 6, 487–500.
Doerffer, R., Schiller, H., 2008. MERIS lake water algorithm for BEAM. ATBD, GKSS Research Center, Geesthacht, Germany. Version 1.0, 10 Jun 08. http://www.brockmann-consult.de/beam-wiki/download/attachments/1900548/meris_c2r_atbd_atmo_20080609_2.pdf?version=1&modificationDate=1213091940000.

Douglas, R.W., Rippey, B., Gibson, C.E., 2002. Interpreting sediment trap data in relation to the dominant sediment redistribution process in a lake. Archives of Hydrobiology 155, 529–539.
Environmental Protection Agency (EPA), 1971. U.S.EPA National Exposure Research Laboratory (NERL) method 160.2. Residue, non-filterable (gravimetric, dried at 103–105). https://www.nemi.gov/apex/f?p=237:38:935723244128883::::P38_METHOD_ID:5213.
Honjo, S., 1996. Fluxes of particles to the interior of the open ocean. In: Ittekkot, V., Schäfer, P., Honjo, S., Depetris, P.J. (Eds.), Particle Flux in the Ocean. John Wiley & Sons, Chichester, pp. 91–154.
Huguet, C., Fietz, S., Stockhecke, M., Sturm, M., Anselmetti, F.S., Rosell-Mele, A., 2011. Biomarker seasonality study in Lake Van, Turkey. Organic Geochemistry 42, 1289–1298.
Kaden, H., Peeters, F., Lorke, A., Kipfer, R., Tomonaga, Y., Karabiyikoğlu, M., 2010. The impact of lake level change on deep-water renewal and oxic conditions in deep saline Lake Van, Turkey. Water Resources Research 64.
Kadioğlu, M., Şen, Z., Batur, E., 1997. The greatest soda-water lake in the world and how it is influenced by climatic change. Annals of Geophysics 15, 1489–1497.
Kelts, K., Shahrabi, M., 1986. Holocene sedimentology of hypersaline Lake Urmia, northwestern Iran. Palaeogeography, Palaeoclimatology, Palaeoecology 54, 105–130.
Kempe, S., 1977. Hydrographie, Warven-Chronologie und Organische Geochemie des Van Sees, Ost-Türkei. Sonderdruck aus Mitteilungen aus dem Geologisch-Paläontologischen Institut der Universität Hamburg, 47, pp. 125–228. Hydrography, varve-chronology and organic geochemistry of Lake Van, east Turkey.
Kempe, S., Kazmierczak, J., Landmann, G., Konuk, T., Reimer, A., Lipp, A., 1991. Largest known microbialites discovered in Lake Van, Turkey. Nature 349, 605–608.
Kienel, U., Schwab, M.J., Schettler, G., 2005. Distinguishing climatic from direct anthropogenic influences during the past 400 years in varved sediments from Lake Holzmaar (Eifel, Germany). Journal of Paleolimnology 33, 327–347.
Lahet, F., Stramski, D., 2010. MODIS imagery of turbid plumes in San Diego coastal waters during rainstorm events. Remote Sensing of Environment 114, 332–344.
Landmann, G., Kempe, S., 2005. Annual deposition signal versus lake dynamics: microprobe analysis of Lake Van (Turkey) sediments reveals missing varves in the period 11.2–10.2 ka BP. Facies 51, 135–145.
Landmann, G., Reimer, A., Lemcke, G., Kempe, S., 1996. Dating Late Glacial abrupt climate changes in the 14,570 yr long continuous varve record of Lake Van, Turkey. Palaeogeography, Palaeoclimatology, Palaeoecology 122, 107–118. doi:10.1016/0031-0182(95)00101-8.
Lemcke, G. 1996. Paläoklimarekonstruktion am Van See (Ostanatolien, Türkei). Ph.D. Thesis. Swiss Federal Institute of Technology Zurich. [Paleoclimate reconstruction at Lake Van (Eastern Anatolia, Turkey).]
Lemcke, G., Sturm, M., 1997. $\delta^{18}O$ and trace element measurements as proxy for the reconstruction of climate changes at Lake Van (Turkey): preliminary results. NATO ASI Series 149, 653–678.
Litt, T., Krastel, S., Sturm, M., Kipfer, R., Örcen, S., Heumann, G., Franz, S.O., Uelgen, U.B., Niessen, F., 2009. Lake Van drilling project PALEOVAN, International Continental Scientific Drilling Program (ICDP), results of a recent pre-site survey and perspectives. Quaternary Science Reviews 28, 1555–1567.
Litt, T., Anselmetti, F.S., Cagatay, M.N., Kipfer, R., Krastel, S., Schmincke, H.-U., Sturm, M., 2011. A 500,000-year-long sediment archive drilled in eastern Anatolia. EOS Transactions, American Geophysical Union 92, 477–479. doi:10.1029/2011EO510002.
Lotter, A.F., Birks, H.J.B., 1997. The separation of the influence of nutrients and climate on the varve time-series of Baldeggersee, Switzerland. Aquatic Sciences 59, 362–375.
Lotter, A.F., Sturm, M., Terranes, J.L., Wehrli, B., 1997. Varve formation since 1885 and high-resolution varve analyses in hypertrophic Baldeggersee (Switzerland). Aquatic Sciences 59, 304–325.
Matthews, M.W., Bernard, S., Winter, K., 2010. Remote sensing of cyanobacteria-dominant algal blooms and water quality parameters in Zeekoevlei, a small hypertrophic lake, using MERIS. Remote Sensing of Environment 114, 2070–2087.
Meyers, P.A., Teranes, J.L., 2001. Sediment organic matter. In: Last, W.M., Smol, J.P. (Eds.), Tracking Environmental Change Using Lake Sediments — Physical and Geochemical Methods, Vol. 2. Kluwer Academic Publishers, Dordrecht, The Netherlands.
Odermatt, D., Giardino, C., Heege, T., 2009. Chlorophyll retrieval with MERIS Case-2-regional in perialpine lakes. Remote Sensing of Environment 11, 607–617.
Ohlendorf, C., Sturm, M., 2008. A modified method for biogenic silica determination. Journal of Paleolimnology 39, 137–142.
Reimer, A., Landmann, G., Kempe, S., 2008. Lake Van, Eastern Anatolia, hydrochemistry and history. Aquatic Geochemistry 15, 195–222.
Roberts, N., Wright, H.E., 1993. Vegetational, lake-level, and climatic history of the near east and Southwest Asia. In: Wright, H.E., Kutzbach, J.E., Webb III, T., Ruddimann, W.F., Street-Perrott, F.A., Bartlein, P.J. (Eds.), Global Climates Since the Last Glacial Maximum. University of Minnesota Press, pp. 194–220.
Ruiz-Verdú, R., Koponen, S., Heege, T., Doerffer, R., Brockmann, C., Kallio, K., Pyhälahti, T., Pena, R., Polvorionos, A., Heblinski, J., Ylöstalo, P., Conde, L., Odermatt, D., Estelles, V., Pulliainen, J., 2008. Development of MERIS lake water algorithms: validation results from Europe. 2nd MERIS/AATSR workshop, Frascati, Italy, 22 Sep 08–26 Sep 08. http://www.brockmann-consult.de/beam-wiki/download/attachments/8355860/MERIS_LAKES_Validation_report.pdf.
Santer, R., Zagolski, F., 2009. ICOL — Improve contrast between ocean and land. ATBD, Université du Littoral, Wimereux, France. Version 1.1, 6 Jan 09. http://www.brockmann-consult.de/beam-wiki/download/attachments/13828113/ICOL_ATBD_1.1.pdf?version=1&modificationDate=1231230197000.
Sengör, A.M.C., Görür, N., Saroglu, F., 1986. Strike-slip faulting and related basin formation in zones of tectonic escape: Turkey as a case study. In: Biddle, K.D., Christie-Blick, N. (Eds.), Strike-slip Deformation, Basin Formation and Sedimentation: Special Publication — Society of Economic Paleontologists and Mineralogists, pp. 227–264.
Shinn, E.A., Steinen, R.P., Lidz, B.H., Swart, P.K., 1989. Perspectives: whitings, a sedimentological dilemma. Journal of Sedimentary Petrology 59, 147–161.
Stabel, H.H., 1986. Calcite precipitation in Lake Constance: chemical equilibrium, sedimentation, and nucleation by algae. Limnology and Oceanography 31, 1081–1093.
Stavn, R.V., Rick, H.J., Falster, A.V., 2009. Correcting the errors from variable sea salt retention and water of hydration in loss on ignition analysis: implications for studies of estuarine and coastal waters. Estuarine, Coastal and Shelf Science 81, 575–582.
Stockhecke, M., 2008. The Annual Particle Cycle of Lake Van: Insights From Space, Sediments and the Water Column. M.S. Thesis. University of Zurich.
Stramski, D., Babin, M., Woźniak, S.B., 2007. Variations in the optical properties of terrigenous mineral-rich particulate matter suspended in seawater. Limnology and Oceanography 52, 2418–2433.
Strong, A.E., Eadie, B.J., 1978. Satellite observations of calcium carbonate precipitation in the Great Lakes. Limnology and Oceanography 23, 877–887.
Sturm, M., Zeh, U., Müller, J., Sigg, L., Stabel, H.-H., 1982. Schwebstoffuntersuchungen im Bodensee mit Intervall-Sedimentationsfallen. Eclogae Geologicae Helvetiae 15/3, 579–588.
Teranes, J.L., McKenzie, J.A., Bernasconi, S.M., Lotter, A.F., Sturm, M., 1999. A study of oxygen isotopic fractionation during bio-induced calcite precipitation in eutrophic Baldeggersee, Switzerland. Geochimica et Cosmochimica Acta 63, 1981–1989.
Thompson, J.B., Schultze-Lam, S., Beveridge, T.J., Des Marais, D.J., 1997. Whiting events: biogenic origin due to the photosynthetic activity of cyanobacterial picoplankton. Limnology and Oceanography 42, 133–141.
Thunell, R., Pride, C., Tappa, E., Muller-Karger, F., 1993. Varve formation in the Gulf of California: insights from time series sediment trap sampling and remote sensing. Quaternary Science Reviews 12, 451–464. doi:10.1016/S0277-3791(05)80009-5.